

# Entanglement, Subsystem Particle Numbers and Topology in Free Fermion Systems

Y. F. Zhang<sup>1</sup>, L. Sheng<sup>1</sup>, R. Shen<sup>1</sup>, Rui Wang<sup>1 2</sup>, D. Y. Xing<sup>1</sup>

<sup>1</sup>National Laboratory of Solid State Microstructures and Department of Physics, Nanjing University, Nanjing 210093, China

<sup>2</sup>Department of Physics, Zhejiang Ocean University, Zhoushan 316000, China

E-mail: shengli@nju.edu.cn

**Abstract.** We study the relationship between bipartite entanglement, subsystem particle number and topology in a half-filled free fermion system. It is proposed that the spin-projected particle numbers can distinguish the quantum spin Hall state from other states, and can be used to establish a new topological index for the system. Furthermore, we apply the new topological invariant to disordered system and show that a topological phase transition occurs when the disorder strength is increased beyond a critical values. It is also shown that the subsystem particle number fluctuation displays behavior very similar to the entanglement entropy. It provides a lower-bound estimation for the entanglement entropy, which can be utilized to obtain an estimate of the entanglement entropy experimentally.

## 1. Introduction

Topological phases of matter are usually distinguished by using some global topological properties, such as topological invariants and topologically protected gapless edge modes, rather than certain local order parameters. The integer quantum Hall effect [1], fractional quantum Hall effect [2], and band Chern insulators [3] can be characterized by Chern numbers or Berry phases [4,5]. The quantum spin Hall (QSH) effect [6,7] and the three-dimensional topological insulators [8,9] are characterized by the  $Z_2$  invariant [10] or spin Chern number [11,12]. In recent years, quantum entanglement [13], which reveals the phase information of the quantum-mechanical ground-state wavefunction, has been used as a tool to characterize the topological phases. As shown by Levin and Wen [14] and also by Kitaev and Preskill [15], the existence of topological entanglement entropy in a fully gapped system, such as fractional quantum Hall [17] and the gapped  $Z_2$  spin liquid [14,16], indicates existence of long-range quantum entanglement (topological order [18] in equivalent parlance). Interestingly, a very recent work [19] proved that topological order can also be read and assessed by the geometric entanglement in multipartite entangled systems. Another important progress is the demonstration that the entanglement spectrum (ES) [20] reveals the gapless edge spectrum for fractional quantum Hall systems [20–24], Chern insulators [25,26], topological insulators [27–29] and even to spin systems [30–32].

Supposing  $A$  and  $B$  to be two blocks of a large system in a pure quantum state, the reduced density matrix (RDM)  $\rho_A$  can be obtained by tracing over degrees of freedom of  $B$ . Then the Von Neumann entanglement entropy (EE) can be computed

$$S_{ent} = -\text{tr}(\rho_A \ln \rho_A) = -\text{tr}(\rho_B \ln \rho_B) . \quad (1)$$

It has been shown that for bipartite subsystems  $A$  and  $B$  with a smooth boundary,  $S_{ent}$  has the form of  $S_{ent} = \alpha L - S_{top}$ , where  $L$  is the length of the boundary,  $\alpha$  is a non universal coefficient, and  $-S_{top}$  is a universal constant called the *topological entanglement entropy* [14,15]. Moreover, if we write the RDM in the form of  $\rho_A = \exp(-H_{ent})/Z$ , where  $Z$  is a normalization constant, and  $H_{ent}$  is known as the *entanglement Hamiltonian*, the eigenvalue spectrum  $\{\varepsilon_i\}$  of  $H_{ent}$  is called the ES, which stores more information about the quantum entanglement than the EE [20].

In this paper, we study the relationship between bipartite entanglement and subsystem particle number in half-filled free fermion systems. It was proposed in Ref. [33], for systems with translational invariance in one dimension, the discontinuity in the subsystem particle number as a function of the conserved momentum indicates whether or not the ES has a spectral flow, which is determined by the topological invariant of the system [29]. Nevertheless, this approach has an exceptional case for a half-filled QSH system with two-dimensional inversion symmetry. To overcome the inadequacy, we define spin-projected particle numbers, based on which spin trace indices can be well defined, for the QSH system with or without  $s_z$  conservation. Spin trace indices are univocally related to the topological invariant of QSH system, i.e., the  $Z_2$  index. Furthermore, we show that spin trace indices will still work well in disordered



**Figure 1.** (Color online) Schematic view of a cylinder and a torus. The entanglement cuts divide the system into two equal parts  $A$  and  $B$ . For the cylinder geometry, the entanglement cut leads to one interface (a); and for the torus geometry, the cuts lead to two interfaces (b).

systems and can demonstrate a topological phase transition. We further investigate the relationship between the EE and subsystem particle number fluctuation. The latter is also dominated by the boundary excitations of the system, and satisfies a similar area law as the EE.

In the next section, we introduce the model Hamiltonian, and explain the procedure to calculate the ES and EE. In Sec. III, numerical calculation of the ES is carried out, and the connection between the subsystem spin-projected particle numbers and the topological invariants in different phases is established. In Sec. IV, we apply spin trace indices to disorder system and show it can demonstrate the phase transition from the QSH to the trivial insulator. In Sec. V, the relationship between the EE and subsystem particle number fluctuation is discussed. Our results are summarized and discussed in the final section.

## 2. MODEL HAMILTONIAN

We begin with the tight-binding model Hamiltonian for the QSH system introduced by Kane and Mele [6, 10], plus an additional exchange field [36]

$$\begin{aligned}
 H = & - \sum_{\langle i, j \rangle} c_i^\dagger c_j + i v_{so} \sum_{\langle\langle i, j \rangle\rangle} c_i^\dagger \sigma_z v_{ij} c_j \\
 & + i v_r \sum_{\langle i, j \rangle} c_i^\dagger (\sigma \times \mathbf{d}_{ij})_z c_j + \sum_i m_i c_i^\dagger c_i + g \sum_i c_i^\dagger \sigma_z c_i .
 \end{aligned} \tag{2}$$

Here, the first term is the usual nearest neighbor hopping term with  $c_i^\dagger = (c_{i,\uparrow}^\dagger, c_{i,\downarrow}^\dagger)$  as the electron creation operator on site  $\mathbf{i}$ , where the hopping integral is set to be unity. The second term is the intrinsic spin-orbit coupling (SOC) with coupling strength  $v_{so}$ , where  $\langle\langle \mathbf{i}, \mathbf{j} \rangle\rangle$  stands for the second nearest neighbor sites, and  $v_{ij} = (\mathbf{d}_{kj} \times \mathbf{d}_{ik})_z / |(\mathbf{d}_{kj} \times \mathbf{d}_{ik})_z|$ . Here,  $\mathbf{k}$  is the common nearest neighbor of  $\mathbf{i}$  and  $\mathbf{j}$ , and vector  $\mathbf{d}_{ik}$  points from  $\mathbf{k}$  to  $\mathbf{i}$ .  $v_{ij} = +1$  for counter-clockwise hopping, and  $v_{ij} = -1$  otherwise.  $\sigma_z$  is a Pauli matrix describing the electrons spin. The intrinsic SOC opens a band gap and drives the system into the QSH phase. The third term stands for the nearest neighbor Rashba SOC with  $\sigma$  the Pauli matrix, and  $v_r$  is Rashba SOC strength. The intrinsic SOC term breaks the

$SU(2)$  symmetry down to  $U(1)$ , and the Rashba SOC term breaks the remaining  $U(1)$  spin symmetry down to  $Z_2$ . The fourth term stands for a staggered sublattice potential ( $m_i = \pm m$ ), which also opens a gap at the Dirac point but drives the system into a trivial topology phase. The last term represents a uniform exchange field with strength  $g$ , which explicitly violates the time reversal symmetry.

We consider systems with cylinder or torus boundary conditions, consisting of  $N_x$  ( $N_x$  to be even) zigzag chains along the circumferential direction ( $y$  direction). The size of the sample will be denoted as  $N = N_x \times N_y$  with  $N_y$  as the number of atomic sites on each chain. We perform the entanglement cut along the  $y$  direction, which results in one or two interfaces between the two equal parts  $A$  and  $B$ , respectively, for the cylinder or torus geometry, as shown in Fig. 1. In order to examine the EE and ES, an Schmidt decomposition on the ground-state wavefunction or calculation of the RDM is usually needed. For non-interacting fermion systems, however, the necessary information of the entanglement can also be obtained from the following two-point correlators [37]

$$c_{\tau_1, \tau_2}(\mathbf{i}, \mathbf{j}) = \langle c_{i, \tau_1}^\dagger c_{j, \tau_2} \rangle. \quad (3)$$

Here,  $\langle \cdot \rangle$  means the ground-state expectation of an operator.  $\tau$  can be an index of spin, pseudospin, or orbital degree of freedom.

Using the Fourier transformation (FT) along the  $y$  direction, the Hamiltonian can be rewritten as  $H = \sum_{k_y, i, j} c_i^\dagger(k_y) h_{i, j}(k_y) c_j(k_y)$ , where  $c_i^\dagger(k_y) = (c_{i, \uparrow}^\dagger(k_y), c_{i, \downarrow}^\dagger(k_y))$  are the electron creation operators. After performing the entanglement cut, we treat part  $A$  as the subsystem, and trace out the degrees of freedom of  $B$ . It should be noted that any of the correlators  $c_{\tau_1, \tau_2}(\mathbf{i}, \mathbf{j})$  with  $\mathbf{i}$  and  $\mathbf{j}$  confined in  $A$  is unchanged by the tracing. When carrying out the FT on the correlators, we can get

$$c_{\tau_1, \tau_2}(\mathbf{i}, \mathbf{j}) = \frac{1}{N_y} \sum_{k_y} e^{ik_y \cdot (i_y - j_y)} \langle c_{i, \tau_1}^\dagger(k_y) c_{j, \tau_2}(k_y) \rangle, \quad (4)$$

where  $i$  and  $j$  discriminate the zigzag chains. We use  $\langle c_{i, \tau_1}^\dagger(k_y) c_{j, \tau_2}(k_y) \rangle$  to form a hermitian matrix  $\mathcal{C}(k_y)$ . Then the entanglement Hamiltonian is given by [37]

$$H_{ent} = \ln(\mathcal{C}^{-1} - 1). \quad (5)$$

The spectrum  $\{\zeta_i\}$  of  $\mathcal{C}$  is related to spectrum  $\{\varepsilon_i\}$  of  $H_{ent}$  by  $\zeta_i = 1/(e^{\varepsilon_i} + 1)$ , where  $\zeta_i$  acts as the average fermion number in the entanglement energy level  $\varepsilon_i$  at ‘‘temperature’’  $T = 1$ . By using the spectrum of  $\mathcal{C}$ , the EE at each  $k_y$  sector is given by  $s_{ent}(k_y) = \sum_i s_i$ , with

$$s_i = -\zeta_i \ln \zeta_i - (1 - \zeta_i) \ln(1 - \zeta_i). \quad (6)$$

From the viewpoint of probability theory,  $s_i$  in Eq. (6) can be regarded as the Shannon (information) entropy of the Bernoulli distribution, i.e., the  $i$ -th entanglement level  $\varepsilon_i$  has probability  $\zeta_i$  of being occupied while  $(1 - \zeta_i)$  of being unoccupied. As a result,  $S_{ent}$  is the Shannon entropy of a series of such independent Bernoulli distributions. In the following, we will perform systematic numerical simulations to study various phases of Hamiltonian (2) in terms of the ES and the subsystem particle number.

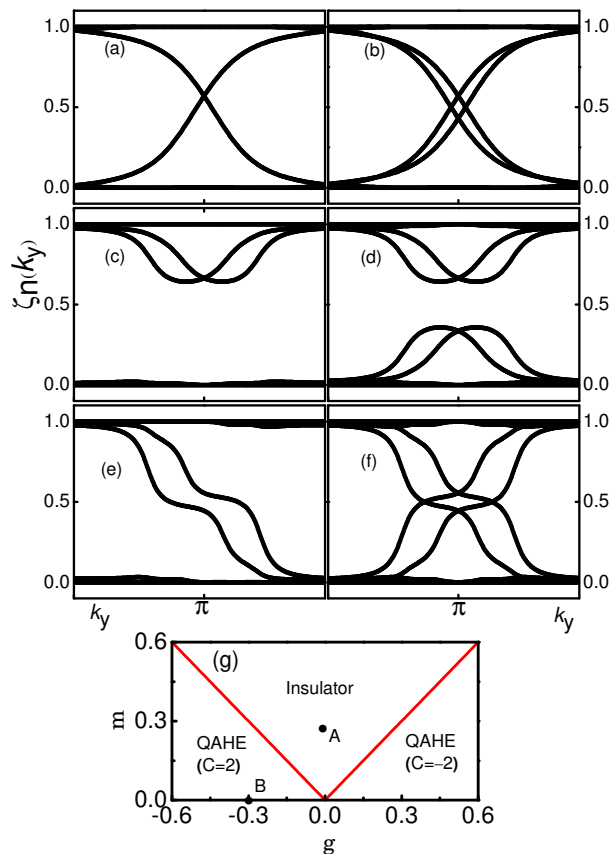


**Figure 2.** (a-f) Single-particle entanglement spectrum in the cylinder geometry (left panels) and torus geometry (right panels) for (a,b) the QSH phase with  $v_{so} = m = 0.2$ ,  $v_r = 0.1$ ,  $g = 0$ , (c,d) the insulator phase with  $v_r = -0.3$ ,  $m = 0.3$ ,  $v_{so} = g = 0$ , and (e,f) the quantum anomalous Hall phase  $v_r = g = -0.3$ ,  $v_{so} = m = 0$ . (g) Phase diagram in the  $m$  versus  $g$  plane for  $v_{so} = 0$  and  $v_r \neq 0$ . Points A and B correspond to the parameter values used in (c,d) and (e,f), respectively.

### 3. Entanglement spectrum and subsystem particle number

At  $g = 0$ , Hamiltonian (2) is the standard Kane-Mele model [6], which is invariant under time reversal symmetry. The system is in a QSH phase when  $|m/v_{so}| < [9 - \frac{3}{4}(v_r/v_{so})^2]$ , and is an insulator when  $|m/v_{so}| > [9 - \frac{3}{4}(v_r/v_{so})^2]$ . On the other hand, if we set  $v_{so} = 0$ ,  $v_r$  and  $g$  nonzero, a middle band gap opens when  $|g| \neq |m|$ . The system is in a quantum anomalous Hall phase with Chern number  $C = \pm 2$  [36] for  $|g| < |m|$ , and is an insulator for  $|g| > |m|$ . The band gap closes at the transition point  $|g| = |m|$ . The phase diagram for  $v_{so} = 0$  and  $v_r \neq 0$  is plotted in Fig. 2(g).

Figs. 2(a) and (b) show the ES for the QSH phase, Figs. 2(c) and (d) for the insulator phase, and Figs. 2(e) and (f) for the quantum anomalous Hall phase. Here, it should be emphasized that the nontrivial topological phases exhibit gapless ES [Figs. 2(a), (b), (e), and (f)], corresponding to physical gapless edge modes, and this property is named as the *spectral flow* [29], which has been explained by Qi and his coworkers

for coupled conformally invariant subsystems with left- and right-moving particles in all chiral topological systems [26]. However, the spectral flow is broken for the topologically trivial phase [Figs. 2(c) and (d)], which is also consistent with the property of the correspondent edge states.

In a recent work [33], the authors proposed a new characteristic quantity called the “trace index” to describe topological invariants, which is defined through a subsystem particle number operator  $N_A(k_y) = \sum_{i \in A} c_{i,k_y}^\dagger c_{i,k_y}$ . The expectation of  $N_A(k_y)$  is given by

$$\langle N_A(k_y) \rangle = \langle GS | \sum_{i \in A} c_i^\dagger(k_y) c_i(k_y) | GS \rangle = \text{Tr} \mathcal{C} . \quad (7)$$

In Fig. 3, we plot the expectation of  $N_A(k_y)$  for the three different phases mentioned above. In the cylinder geometry,  $N_A(k_y)$  is discontinuous at some discrete momenta in the nontrivial topological phases, as shown in Figs. 3(a) and (c). This is in contrast to the normal insulator phase [see Fig. 3(b)], where  $N_A(k_y)$  is a continuous function of  $k_y$ . In the torus geometry,  $N_A(k_y)$  is exactly equal to half of the total particle number in the  $k_y$  sector, without showing any discontinuity, because the change of the particle number in  $A$  around interface  $I$  is just canceled by that around interface  $II$  due to the rotation invariance of the torus. In the cylinder geometry, the *trace index* was defined as the total discontinuities of  $\langle N_A(k_y) \rangle$  with varying momentum. Alexandradinata, Hughes, and Bernevig [33] presented a detailed analysis and proved that the trace index is equivalent to the Chern number (or  $Z_2$  invariant) for the Chern ( $Z_2$ ) insulators. Therefore, the subsystem particle number provides a new alternative tool to reveal the topological invariants.

However, as mentioned in Ref. [33], there is an exceptional case in which the subspace of the occupied bands at the symmetric momenta is not closed under time reversal in the ground state. If at the symmetric momenta the Kramers’ doublet that extends along the edge of  $A$  is singly-occupied,  $\langle N_A(k_y) \rangle$  is continuous, even when the system is in a nontrivial topological phase. For the half-filled system under consideration, an exception still happens. While the two-dimensional inversion symmetry remains unchanged ( $m = 0$ ),  $N_A(k_y)$  becomes continuous, as shown in Fig. 3(d). This is because the Kramers’ partners extending along the edge simultaneously cross the Fermi level at the symmetric momentum ( $k_y = \pi$ ) and have opposite contributions to the discontinuities of  $\langle N_A(k_y) \rangle$ .

To overcome this difficulty, we define a new quantity named spin trace index. We choose operator  $P s_z P$  to split the fiber bundle of the occupied states into two bundles with well-defined Chern numbers, where  $P$  is the ground state projector. At half filling and in the presence of time reversal symmetry ( $g = 0$ ),  $P s_z P$  is always a time-odd operator ( $T P s_z P T^{-1} = -P s_z P$ ), so that the spectrum of  $P s_z P$  is symmetric in respect to the origin. As a result, we can use eigenvectors of operator  $P s_z P$  corresponding to the positive (negative) eigenvalues to split the Hilbert space spanned by the occupied-states wave functions into two sub-space (“spin-up” and “spin-down” sub-spaces). The new wave functions for the two sectors are unitary transformation of the original occupied-

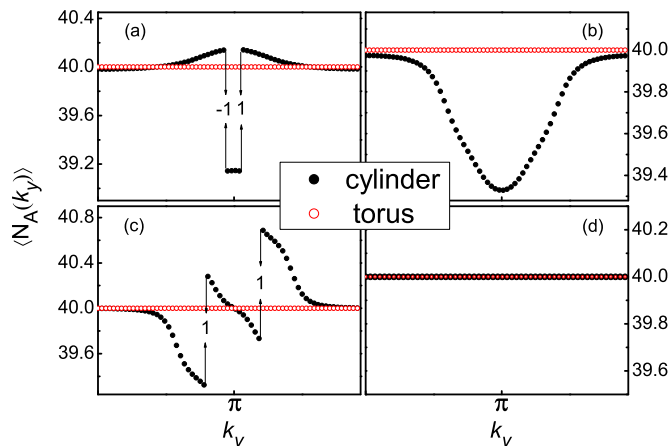


**Figure 3.** (Color online) (a-c) The subsystem particle number in the cylinder geometry and torus geometry for (a) the QSH phase, (b) the insulator phase, and (c) the quantum anomalous Hall phase with all the parameters as same as Fig. 2. (d) The subsystem particle number in the cylinder geometry and torus geometry for the QSH phase with  $v_{so} = v_r = 0.2$ , where the two-dimensional inversion symmetry is retained. Discontinuities in the expectation of the particle number can be observed only in the cylinder geometry.

band wave functions. This splitting results in a smooth decomposition

$$P(k_y) = P^+(k_y) \oplus P^-(k_y), \quad (8)$$

for all  $k_y \in (0, 2\pi]$ , with  $\alpha = \pm$  corresponding to the positive and negative sectors. Straightforwardly, the two-point correlator matrix can also be decomposed into  $\mathcal{C}(k_y) = \mathcal{C}^+(k_y) \oplus \mathcal{C}^-(k_y)$ . It will be shown below that the traces of  $\mathcal{C}^\pm$ , called the *spin-projected subsystem particle numbers*, are related to the topological invariants.

If  $\text{Tr}\mathcal{C}^\alpha(k_y)$  is discontinuous at some momenta  $\{k_{dis}\}$  with  $k_{dis} \in (0, 2\pi]$ , we can define the *spin trace indices* as the total discontinuity, i.e., difference between the limits of  $\text{Tr}\mathcal{C}^\alpha(k_y)$  from right and left in the thermodynamic limit,

$$A^\alpha \equiv \sum_{k_{dis}} \left( \lim_{k \rightarrow k_{dis}^+} \text{Tr}\mathcal{C}^\alpha(k) - \lim_{k \rightarrow k_{dis}^-} \text{Tr}\mathcal{C}^\alpha(k) \right). \quad (9)$$

When the Hamiltonian commutes with  $s_z$  ( $v_r = 0$ ), operator  $P s_z P = I \otimes \sigma_z$ . In this case, the spin trace index are equivalent to the result obtained by calculating  $\sum_i \langle \varphi_i(k_y) | (1 \pm \sigma_z) / 2 | \varphi_i(k_y) \rangle$ , where  $\varphi_i$  are limited to the occupied-band wave functions. In the presence of the Rashba spin-orbit coupling, the matrix form of  $P s_z P$  is no longer diagonal, and thence upper and lower projected spin spectral bands then begin to communicate. Nevertheless, even in this case, it can be confirmed that the two bands are always separated by a finite band gap [34], hence allowing us to define  $A^\alpha$  unambiguously. Based on the splitting principle [35], the two sub-space got through linear combination still have well-defined Chern number. It has been proved that the Chern numbers for the two sectors are topological invariants protected by the energy

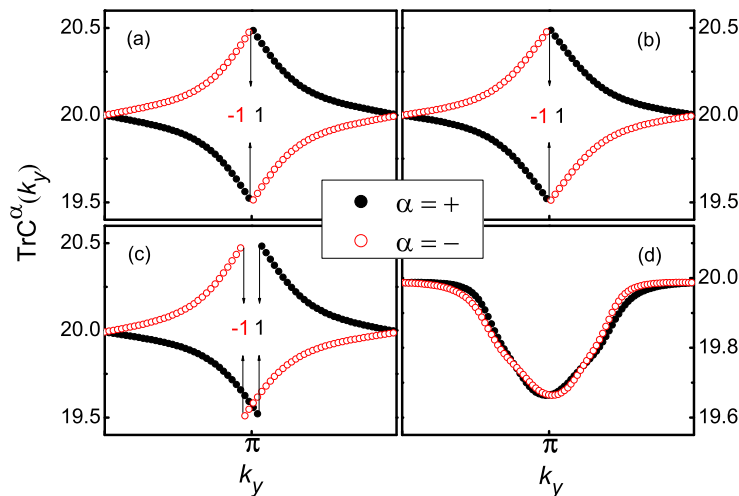


**Figure 4.** (Color online) Subsystem spin-projected particle numbers in the cylinder geometry for the QSH phase (a-c) with  $g = 0$  and different parameters: (a)  $v_{so} = 0.2$  and  $v_r = m = 0$ , (b)  $v_{so} = v_r = 0.2$  and  $m = 0$ , (c)  $v_{so} = m = 0.2$  and  $v_r = 0.1$ , and for the insulator phase (d) with  $v_{so} = v_r = 0.05$ ,  $m = 0.5$  and  $g = 0$ .

gap and spin spectrum gap [12]. Then each sector is an analogy of the quantum Hall system with Chern number  $+1$  or  $-1$ . The Chern number and trace index for a Chern insulator are equivalent to each other [33]. Naturally,  $A^\alpha$  is equivalent to the Chern numbers for each sector. From the quantized Chern number for each sector, it follows that the spin trace index is also quantized, both of them coming from the bulk topology. Then  $Z_2$  index can be defined as the parity of  $A^\alpha$  (for any  $\alpha$ ),

$$A_{Z_2} \equiv A^\alpha \text{ mod } 2, \quad (10)$$

which labels the topologically distinct phases.

We plot  $\text{TrC}^\alpha$  ( $\alpha = \pm$ ) as functions of  $k_y$  in Fig. 4. No matter whether  $s_z$  is conserved, both  $\text{TrC}^+(k_y)$  and  $\text{TrC}^-(k_y)$  show discontinuities at  $k_y = \pi$  with  $A^+ = 1$  and  $A^- = -1$  in the QSH phase [Figs. 4(a) and (b)], where the two-dimensional inversion symmetry is present ( $m = 0$ ). Figure 4(c) shows the discontinuities of  $\text{TrC}^+(k_y)$  and  $\text{TrC}^-(k_y)$  in the QSH phase in which  $s_z$  is not conserved ( $v_r \neq 0$ ) and the two-dimensional inversion symmetry is broken ( $m \neq 0$ ). In this case, the spin trace indices are equal to 1 and  $-1$ , respectively, contributed by two different momentum points. But, in contrast, both  $\text{TrC}^+(k_y)$  and  $\text{TrC}^-(k_y)$  are the continuous functions in the normal insulator phase [Fig. 4(d)]. Consequently, it is easy to get  $A_{Z_2} = 1$  for QSH phase [Figs. 4(a-c)] and  $A_{Z_2} = 0$  for insulator phase [Figs. 4(d)]. Therefore, the subsystem particle number expectation can be used to characterize the topological invariants. Especially, for the QSH systems, the spin trace indices are new well-defined quantities that can reveal the  $Z_2$  invariant and distinguish different quantum phases.



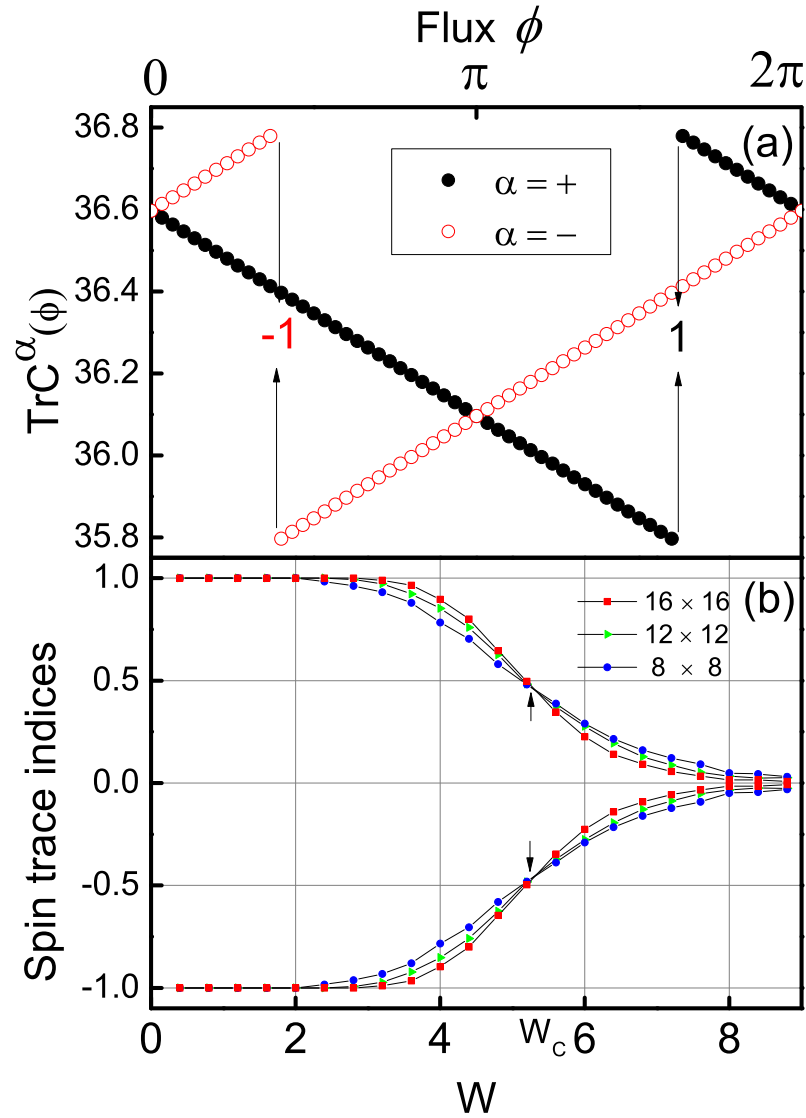


**Figure 5.** (Color online) Disordered spin trace indices for the QSH phase with  $v_{so} = m = 0.2$  and  $v_r = 0.1$ . (a):  $\text{Tr}C^\alpha(\phi)$  as a function of flux  $\phi$  for one time disorder configuration with disorder strength parameter  $W = 0.5$  for sample size  $N = 12 \times 12$ ; (b) Disordered trace indices as a function of the disorder strength parameter  $W$ . The result is averaged over 400 disorder configurations, for several different sample sizes.

#### 4. Application of spin trace indices to disordered system

The spin trace indices can be used for classifying different topological phases, but it will be equally important to extract nontrivial physical consequences from its remarkable properties, in particular, to say something about the localization of the bulk states in the presence of disorder. To study the disorder effect, we include into Hamiltonian (2) a random on-site potential of the form  $\sum_i \omega_i c_i^\dagger c_i$ , with  $\omega_i$  randomly distributed between  $[-W/2, W/2]$ .

We define spin trace indices for systems with translational invariance in one

dimension, but momentum  $k_y$  is no longer a good quantum number in the presence of disorder. However, by introducing a flux inserted through the symmetry axis of the cylinder, we add a parameter  $\phi$  into the Hamiltonian in order to replace the momentum  $k_y$ . Then if  $\text{Tr}\mathcal{C}^\alpha(\phi)$  is discontinuous at some pseudo-momenta  $\{\phi_{dis}\}$  with  $\phi_{dis} \in (0, 2\pi]$ , we can redefine the disordered spin trace indices as:

$$A_\phi^\alpha \equiv \sum_{\phi_{dis}} \left( \lim_{\phi \rightarrow \phi_{dis}^+} \text{Tr}\mathcal{C}^\alpha(\phi) - \lim_{\phi \rightarrow \phi_{dis}^-} \text{Tr}\mathcal{C}^\alpha(\phi) \right). \quad (11)$$

Numerical calculation of the disordered spin trace indices is carried out for a disordered system with  $v_{so} = m = 0.2$  and  $v_r = 0.1$  at half filling, and the results are shown in Fig. 5. In Fig.5(a), we plot  $\text{Tr}\mathcal{C}^\alpha(\phi)$  as a function of flux  $\phi$  for one time disorder configuration with weak disorder  $W = 0.5$ , for sample size  $N = 12 \times 12$ . It is apparent that for weak disorder, the  $\text{Tr}\mathcal{C}^\alpha$  ( $\alpha = \pm$ ) as a function of  $\phi$  behave very similar to the  $\text{Tr}\mathcal{C}^\alpha$  ( $\alpha = \pm$ ) as a function of  $k_y$  which have been showed in Fig. 4. For the QSH, both  $\text{Tr}\mathcal{C}^\alpha$  have only one discontinuous momentum or pseudo-momentum point with discontinuity  $\pm 1$ , which implies the spin trace indices are equal to 1 and  $-1$ , respectively. When the disorder strength  $W$  is increasing,  $\text{Tr}\mathcal{C}^\alpha(\phi)$  become discontinuous at some more pseudo-momenta  $\{\phi_{dis}\}$  points and the calculated spin trace indices as a function of disorder strength after average over 400 times disorder configurations is plotted in Fig. 5(b) with different sample sizes. One can clearly found that the spin trace indices are robust against weak disorder  $W < 2$ . With increasing  $W$  from 2 to 9, the spin trace indices continuously decrease to nearly zero. At the same time, with increasing the sample size, the transition process becomes sharper and sharper, which conforms the expectation that the phase transition from the QSH (with spin trace indices  $\pm 1$ ) to the trivial insulator (with both spin trace indices 0) occurring at around  $Wc \approx 5.2$  should become a sudden drop from  $\pm 1$  to 0 in the thermodynamic limit. In short, as far as disorder goes, loss of translational invariance leads to a loss of the Brillouin zone, and sequentially the  $Z_2$  index can not be defined, so how to abstract the topological invariant from disordered systems becomes very significant. Here the (disordered) spin trace indices we has defined above can be applied to these systems and can display a topological phase transition occuring when the disorder strength is increased beyond a critical values.

## 5. Entanglement entropy and subsystem particle number fluctuation

We have shown that topological properties of the ground state can be extracted from the expectation of subsystem particle number. Now we turn to the variance of  $N_A(k_y)$ . In the past three years, extensive works have been devoted to the study of the relation between the EE and subsystem particle fluctuation for non-topological systems [40]. In this section, we will show that the relation is rather general, it does apply to non-interacting electron systems with a nontrivial band topology. We start from the standard definition of the variance

$$\Delta N_A^2(k_y) = \langle N_A^2(k_y) \rangle - \langle N_A(k_y) \rangle^2. \quad (12)$$

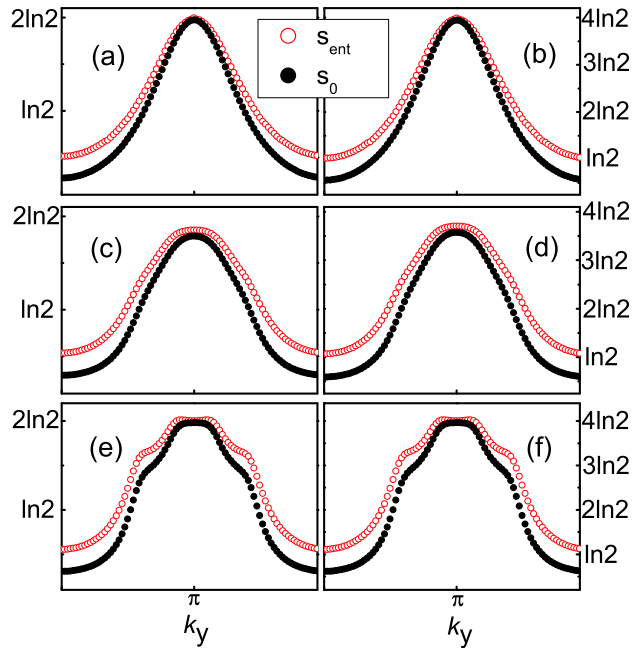


**Figure 6.** (Color online) Entanglement entropy in comparison with subsystem particle number fluctuation for (a-b) the QSH phase, (c-d) the insulator phase, and (e-f) the quantum anomalous Hall phase, in the cylinder geometry (left panels) and torus geometry (right panels). All the parameters are the same as in Fig. 2.

Substituting Eq. (7) into Eq. (12) and using the Wick's theorem to expand all the four-point correlators, one can obtain

$$\begin{aligned} \Delta N_A^2(k_y) &= \sum_{i,j \in A} \langle c_{i,k_y}^\dagger c_{j,k_y} \rangle \langle c_{j,k_y} c_{i,k_y}^\dagger \rangle \\ &= \text{Tr}[\mathcal{C}(1 - \mathcal{C})] , \end{aligned} \quad (13)$$

yielding  $\Delta N_A^2(k_y) = \sum_i \zeta_i(1 - \zeta_i)$ , which is in keeping with the variance formula of the Bernoulli distributions. In order to find a definite relationship between the EE and the variance, one can construct a concave function  $f(x) = -\ln x/(1 - x)$  for  $x \in [0, 1]$ , and apply the Jensen's inequality

$$-x \ln x - (1 - x) \ln(1 - x) \geq (4 \ln 2) \cdot x(1 - x) . \quad (14)$$

The equality holds if and only if  $x = 1/2$ . Equation (14) enables us to make a lower-bound estimation of the EE

$$s_{ent}(k_y) \geq (4 \ln 2) \cdot \Delta N_A^2(k_y) . \quad (15)$$

This inequality is first given in the context of metal [39] and here as a complement, we give a very simple and direct proof. From the inequality one can see that a lower bound of the EE is given by  $s_0(k_y) \equiv (4 \ln 2) \cdot \Delta N_A^2(k_y)$ , which is directly proportional to the particle number fluctuation of subsystem. In Fig. 6, we plot  $s_{ent}(k_y)$  and  $s_0(k_y)$  in the QSH phase, insulator phase, and quantum anomalous Hall phase. In all the cases, the

curves for the particle number fluctuation behave somewhat similarly, and are very close to the corresponding EE. This similarity was observed in the non-topological systems lately [40], and here we find that the similarity remains to hold for the topologically nontrivial system. Moreover, each maximally entangled state with  $\varepsilon_m = 0$  ( $\zeta_m = 1/2$ ) existing only in topology phases contributes a maximal value to the subsystem particle number fluctuation and the EE, which cannot be eliminated by adiabatic continuous deformation, which may provides a new way for the probe of topological insulators.

Furthermore, one can use  $N_A(k_y) = \sum_{i \in A} c_{i,k_y}^\dagger c_{i,k_y}$  to verify  $\Delta N_A^2 = \sum_{k_y} \Delta N_A^2(k_y) \rightarrow \frac{L_y}{2\pi} \int dk_y \Delta N_A^2(k_y)$ , indicating that  $\Delta N_A^2(k_y)$  satisfies a area law [38], similar to the EE,  $S_{ent} = \sum_{k_y} s_{ent}(k_y) \rightarrow \frac{L_y}{2\pi} \int dk_y s_{ent}(k_y)$ . Remarkably, for topologically-ordered states, Ref [19] proved that the non-topologically-ordered term of geometric entanglement obeys a similar area law in multipartite entanglement. We expect that the conclusion should still be true for non-interacting fermions systems. To conclude, the subsystem particle number fluctuation shares several common characteristics with the EE, and so can be utilized to obtain an estimate of the EE. The EE has being widely used in analyzing quantum critical phenomena, topologically ordered states, evolution after a quantum quench, as well as quantum computation [44].

## 6. Summary and discussion

To conclude, we have investigated the relationship between the quantum entanglement and subsystem particle number. The spin trace indices can reveal the topological invariants and be used to classify different phases in QSH systems. This new tool always works well even though  $s_z$  is not conserved. Even in disordered system, it works well and can be used to demonstrate topological phase transition. As to the subsystem particle number fluctuation, it shares several common properties with the EE. They both satisfy the same area law, and are dominated by the boundary excitations with each zero mode having a maximal contribution. The connection between the two quantities is universal, regardless of whether the system has a nontrivial band topology. As a result, the subsystem particle number fluctuation, as an observable quantity, can be utilized to obtain an estimate of the EE experimentally [40].

As long as the Fermi energy still lies in the bulk energy gap, all results that we have obtained will remain about the same. With the Fermi energy lowered into the valence band or increased into the conduction band, the spin trace indices will no longer be quantized and continuously drop from  $\pm 1$  to 0. We also stress that the results obtained in the paper only hold for free fermion systems. Interestingly, as to the entanglement entropy and the subsystem particle number fluctuation, a similar relation has been found for certain types of interacting systems, for example, one dimension quantum spin chains [41], although such a relation is not true for some other interacting systems such as fractional quantum Hall states [42] and two-dimensional spin 1/2 antiferromagnetic Heisenberg model [43].

## Acknowledgments

This work was supported by the State Key Program for Basic Researches of China under grants numbers 2014CB921103 (LS), 2011CB922103 and 2010CB923400 (DYX), the National Natural Science Foundation of China under grant numbers 11225420 (LS), 11304281(RW), 11174125, 91021003 (DYX) and a project funded by the PAPD of Jiangsu Higher Education Institutions.

## References

- [1] Klitzing K V, Dorda G, and Pepper M 1980 *Phys. Rev. Lett.* **45**, 494
- [2] Tsui D C, Stormer H L, and Gossard A C 1982 *Phys. Rev. Lett.* **48**, 1559
- [3] Haldane F D M 1988 *Phys. Rev. Lett.* **61**, 2015
- [4] Thouless D J, Kohmoto M, Nightingale M P, and den Nijs M 1982 *Phys. Rev. Lett.* **49**, 405
- [5] Niu Q, Thouless D J and Wu Y S 1985 *Phys. Rev. B.* **31**, 3372
- [6] Kane C L and Mele E J 2005 *Phys. Rev. Lett.* **95**, 226801
- [7] Bernevig B A, Hughes T L, and Zhang S C 2006 *Science* **314**, 1757
- [8] Hasan M Z and Kane C L 2010 *Rev. Mod. Phys.* **82**, 3045
- [9] Qi X L and Zhang S C 2010 *Physics Today* **63**, 33
- [10] Kane C L and Mele E J 2005 *Phys. Rev. Lett.* **95**, 146802
- [11] Sheng L, Sheng D N, Ting C S, and Haldane F D M 2005 *Phys. Rev. Lett.* **95**, 136602; Sheng D N, Weng Z Y, Sheng L, and Haldane F D M, *Phys. Rev. Lett.* **97**, 036808
- [12] Prodan E 2009 *Phys. Rev. B* **80**, 125327; Prodan E 2010 *New J. Phys.* **12**, 065003
- [13] Amico L, Fazio R, Osterloh A, and Vedral V 2008 *Rev. Mod. Phys.* **80**, 517; Horodecki R, Horodecki P, Horodecki M, and Horodecki K 2009 *Rev. Mod. Phys.* **81**, 865
- [14] Levin M and Wen X G 2006 *Phys. Rev. Lett.* **96**, 110405
- [15] Kitaev A and Preskill J 2006 *Phys. Rev. Lett.* **96**, 110404
- [16] Kitaev A Y 2003 *Ann. Phys.* **303**, 2.
- [17] Haque M, Zozulya O, and Schoutens K 2007 *Phys. Rev. Lett.* **98**, 060401; Zozulya O S, Haque M, Schoutens K, and Rezayi E H 2007 *Phys. Rev. B* **76**, 125310
- [18] Wen X G 2004 *Quantum Field Theory Of Many-body Systems* (New York:Oxford University Press)
- [19] Orus R, Wei T -C , Buerschaper O, Van den Nest M, arXiv:1304.1339v2.(accepted by New Journal of Physics)
- [20] Li H and Haldane F D M 2008 *Phys. Rev. Lett.* **101**, 010504
- [21] Läuchli A M, Bergholtz E J, Suorsa J and Haque M 2010 *Phys. Rev. Lett.* **104**, 156404
- [22] Zaletel M P, Mong R S K , and Pollmann F 2013 *Phys. Rev. Lett.* **110**, 236801
- [23] Tu H H, Zhang Y, Qi X L 2013 *Phys. Rev. B* **88**, 195412
- [24] Cincio L and Vidal G 2013 *Phys. Rev. Lett.* **110**, 067208
- [25] Prodan E, Hughes T L, and Bernevig B A 2010 *Phys. Rev. Lett.* **105**, 115501
- [26] Qi X L, Katsura H, and Ludwig A W W 2012 *Phys. Rev. Lett.* **108**, 196402
- [27] Fidkowski L 2010 *Phys. Rev. Lett.* **104**, 130502
- [28] Hughes T L, Prodan E, and Bernevig B A 2011 *Phys. Rev. B* **83**, 245132
- [29] Fidkowski L, Jackson T S, and Klich I 2011 *Phys. Rev. Lett.* **107**, 036601
- [30] Yao H and Qi X L 2010 *Phys. Rev. Lett.* **105**, 080501
- [31] Pollmann F, Turner A M, Berg E and Oshikawa M 2010 *Phys. Rev. B.* **81**, 064439
- [32] Poilblanc D 2010 *Phys. Rev. Lett.* **105**, 077202
- [33] Alexandradinata A, Hughes T L, Bernevig B A 2011 *Phys. Rev. B.* **84**, 195103
- [34] Inoue J and Tanaka A 2012 *Phys. Rev. B.* **85**, 125425
- [35] Nakahara M 2003 *Geometry, topology and Physics* (Bristol:IOP Publishing) p 429
- [36] Qiao Z, Yang S A, Feng W, Tse W K, Ding J, Yao Y, Wang J, and Niu Q 2010 *Phys. Rev. B.*

- 82**, 161414(R); Yang Y, Xu Z, Sheng L, Wang B G, Xing D Y, and Sheng D N 2011 *Phys. Rev. Lett.* **107**, 066602
- [37] Peschel I 2004 *J. Stat. Mech.* P06004
- [38] Eisert J, Cramer M, and Plenio M B 2010 *Rev. Mod. Phys.* **82**, 277
- [39] Klich I 2006 *J. Phys. A.* **39**, L85
- [40] Song H F, Flindt C, Rachel S, Klich I, and Hur K L 2011 *Phys. Rev. B* **83**, 161408(R); Song H F, Rachel S, Flindt C, Klich I, Lafroncie N and Hur K L 2012 *Phys. Rev. B* **85**, 035409
- [41] Song H F, Rachel S, Flindt C, Klich I 2010 *Phys. Rev. B* **82**, 012405
- [42] Hsu B, Grosfeld E, and Fradkin E 2009 *Phys. Rev. B* **80**, 235412
- [43] Song H F, Lafroncie N, Rachel S, and Hur K L 2011 *Phys. Rev. B* **83**, 224410
- [44] Klich I, Levitor L 2009 *Phys. Rev. Lett* **102**, 100502